Automatic Fascicle Length Estimation on Muscle Ultrasound Images With an Orientation-Sensitive Segmentation

Guang-Quan Zhou and Yong-Ping Zheng*, *Senior Member, IEEE*

Abstract*—*Goal: **The fascicle length obtained by ultrasound imaging is one of the crucial muscle architecture parameters for understanding the contraction mechanics and pathological conditions of muscles. However, the lack of a reliable automatic measurement method restricts the application of the fascicle length for the analysis of the muscle function, as frame-by-frame manual measurement is time-consuming. In this study, we propose an automatic measurement method to preclude the influence of nonfascicle components on the estimation of the fascicle length by using motion estimation of fascicle structures.** ***Methods:*** **The method starts with image segmentation using the cohesiveness of fascicle orientation as a feature, obtaining the fascicle change by tracking manually marked points on the fascicular path with the Lucas–Kanade optical flow algorithm applied on the segmented image.** ***Results:*** **The performance of this method was evaluated on ultrasound images of the gastrocnemius obtained from seven healthy subjects (34.4 ± 5.0 years). Waveform similarity between the manual and dynamic measurements was assessed by calculating the overall similarity with the coefficient of multiple correlations (CMC).** ***In vivo*** **experiments demonstrated that fascicle tracking with the orientation-sensitive segmentation ($CMC = 0.97 \pm 0.01$) was more consistent with the manual measurements than existing automatic methods ($CMC = 0.87 \pm 0.10$).** ***Conclusion:*** **Our method was robust to the interference of nonfascicle components, resulting in a more reliable measurement of the fascicle length.** ***Significance:*** **The proposed method may facilitate further research and applications related to real-time architectural change of muscles.**

***Index Terms*—Effective fascicle region, fascicle length, image segmentation, muscle, optical flow, orientation-sensitive segmentation, ultrasound imaging.**

I. Introduction

MUSCLE imaging is a promising field of research in understanding the biological and bioelectrical characteristics of muscles, as well as assessing their function and pathological conditions through the observation of muscle architectural change, since muscle activation is closely related to its structure [1]. Recently, sonomyography (SMG), representing the real-time change of muscle architecture obtained using ultrasound imaging, has been proposed as a noninvasive option to measure muscle activation under different contractions [2]. It has been reported that the muscle architecture, primarily delineated by the geometric layout of the fascicles within the skeletal muscle, including the fascicle length and the pennation angle, is highly correlated with muscle contraction [3]–[9]. SMG has showed its potential in both diagnosis and rehabilitation assessment *in vivo*, as a reliable research and clinical tool. It has been used to monitor treatment outcomes for patients with motor problems [10], [11], prepare rehabilitation plans for patients with surgical operations [12], [13], and control powered prostheses [14], [15].

Fascicle length is the most often used SMG parameter to quantify changes in the fascicle geometry of muscle. Since the ability of muscle to generate the force is largely determined by its fascicle length, the change of the fascicle length has been examined in response to contraction [16], [17], aging [18], [19], fatigue [20], and physical training [21], [22]. Moreover, modulation of the fascicle–tendinous tissue interaction, which occurs to make the movement more economic via effective utilization of tendinous tissue elasticity for specific movement tasks [23]–[27], can also be estimated from changes of the fascicle and tendon length. This morphometric skeletal muscle parameter is therefore of great importance to understanding the mechanism of muscle contraction. Although the manual measurement of the fascicle length was reported to be reproducible [28], the method is time-consuming and subjective, restricting the application of the fascicle length in the dynamic analysis of the muscle function, especially when dealing with a sequence of ultrasound images. Since fascicles are usually nonuniformly distributed as line-like structures in ultrasound images [5], [29], some automatic fascicle detection approaches based on the Hough or Radon transforms [30]–[32] have been proposed for estimating the fascicle length. However, the fascicle structures are often obscured by speckle noise, making it difficult to locate them accurately. Moreover, intramuscular blood vessels are also visible as line-like structures in the fascicle region of some ultrasound images [33], [34], resulting in incorrect measurements of the fascicle length.

Motion between successive images has also been used to estimate the fascicle length by observing the continuous changes in the fascicle region [34]–[38]. Under the assumption that homogeneous affine transformations are applicable in the muscle region, Cronin, *et al*. [36] estimated global affine transform parameters with the Lucas–Kanade optical flow algorithm [39], by regarding a selected fascicle region as a whole patch to derive

Manuscript received March 12, 2015; revised May 18, 2015; accepted June 9, 2015. Date of publication June 16, 2015; date of current version November 20, 2015. This work was partially supported by the Hong Kong Polytechnic University (G-YL74) and the Research Grant Council of Hong Kong (PolyU 152220/14E). *Asterisk indicates corresponding author.*

G.-Q. Zhou is with the Interdisciplinary Division of Biomedical Engineering, Hong Kong Polytechnic University.

*Y.-P. Zheng is with the Interdisciplinary Division of Biomedical Engineering, Hong Kong Polytechnic University, Hung Hom, Hong Kong (e-mail: ypzheng@ieee.org).

Color versions of one or more of the figures in this paper are available online at http://ieeexplore.ieee.org.

Digital Object Identifier 10.1109/TBME.2015.2445345

0018-9294 © 2015 IEEE. Personal use is permitted, but republication/redistribution requires IEEE permission.
See http://www.ieee.org/publications_standards/publications/rights/index.html for more information.

Authorized licensed use limited to: COLORADO SCHOOL OF MINES. Downloaded on July 16,2021 at 21:17:52 UTC from IEEE Xplore. Restrictions apply.

the changes in the fascicle length. Based on the assumption of straight fascicles, the fascicle length was identified by calculating the displacement of predefined points on the fascicular path using the global affine transform parameters. In this approach, the accumulation of errors in tracking small regions of interest (ROI) was avoided by estimating global movement over a large region [38]. Nonetheless the nonfascicle components of speckle noise that can violate the assumption of homogeneous affine transformations were not taken into account which could lead to inaccurate estimation of the fascicle length in some images. Using the framework of Bayesian multiple hypotheses, the Kanade–Lucas–Tomasi (KLT) feature trackers [40] combined with visible fascicle structures have also been proposed to estimate the changing fascicle shape [37]. About 200 nonoverlapping square feature templates with a size 15×15 pixels, derived in the fascicle region using multiresolution active shape model training, were tracked using KLT weighted by a multiscale vessel enhancement map [41]. This map was used to obtain global fascicle displacements and changes of the fascicle length with the particle filter, thus allowing recovery from small tracking errors. However, the weight of nonfascicle components, such as visible intramuscular blood vessels, was also increased in the calculation, possibly influencing the estimation of the fascicle length. Moreover, the time-consuming multiresolution active shape model segmentation and particle filter also restricted the application of this approach.

In this study, under the assumption of homogeneous affine transformations, we propose an automatic method for estimating the change of the fascicle length in consecutive ultrasound images by calculating global affine transform parameters over the effective fascicle region obtained with an orientation-sensitive segmentation algorithm, in order to address the limitations of currently available approaches. The orientation-sensitive segmentation algorithm was designed to segment visible fascicle structures from the whole muscle region based on the observation of similar orientations of fascicles in muscles. The automatic method for fascicle length estimation is described in detail in Section II, and was tested with real ultrasound image sequences of the human gastrocnemius (GM) during cyclic plantar flexion.

II. Methods

Based on the observation of similar fascicular orientations in muscle ultrasound images [42], the region containing the visible fascicle structure, termed as the effective fascicle region, can be derived from the whole ultrasound image using our orientation-sensitive segmentation algorithm described in Section II-A. Under the assumptions of straight fascicles and homogeneous affine transformations, the global affine transform parameters were then estimated between consecutive images from the Lucas–Kanade optical flow algorithm [39] over the effective fascicle region. The flowchart of our proposed method is illustrated in Fig. 1. After the displacement of the predefined points on the fascicular path were calculated from the global affine transform parameters, the fascicle length was then derived as the distance along the fascicular path from the superficial aponeurosis to the deep aponeurosis. In cases where the fascicle extended beyond the view of the image, the whole fascicle length was estimated by linearly extrapolating both the paths of the fascicles and the aponeuroses.

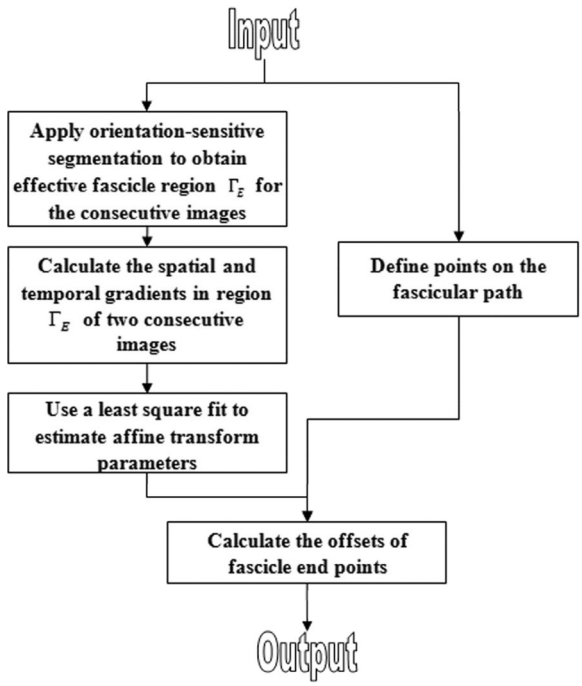

Fig. 1. Flowchart of the proposed tracking algorithm.

A. Effective Fascicle Region Segmentation

The fascicle region in the ultrasound image contains patterns of ridges and valleys, similar to that of a fingerprint image. However, the image speckles often disguise these ridges and valleys increasing the difficulty of accurate fascicle recognition. Fig. 2(a) shows a typical GM ultrasound image containing parallel fascicles with speckle noise. Moreover, the visible nonfascicle components in the muscle such as intramuscular blood vessels [33], [34], having completely different orientations from the fascicles, would also affect fascicle identification. Fig. 3(a) shows an example of a GM ultrasound image with visible intramuscular blood vessels. Motivated by the similar fascicular orientations in muscle ultrasound images and images for fingerprint enhancement [43], the primary local orientation calculated using an intensity gradient [44] could be used to identify the effective fascicle region for the estimation of the fascicle length. An orientation-sensitive segmentation algorithm was then designed with a set of intermediate steps applied on the input ultrasound image to obtain the effective fascicle region. As shown in Fig. 4, the main steps of the algorithm included.

1) *Normalization*: An input image was normalized with mean $= 0$ and variance $= 1$.
2) *Local orientation estimation*: The local orientation was estimated from the normalized image to form a local orientation map.

Authorized licensed use limited to: COLORADO SCHOOL OF MINES. Downloaded on July 16,2021 at 21:17:52 UTC from IEEE Xplore. Restrictions apply.

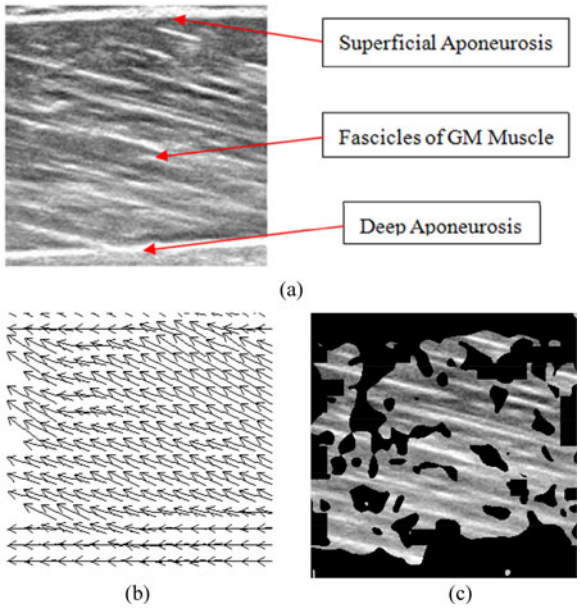

Fig. 2. Example of segmentation for the ultrasound image containing parallel fascicles with speckle noise. (a) Original GM ultrasound image containing parallel fascicles with speckle noise. (b) Orientation flow of the image. (c) Orientation-sensitive segmentation result.

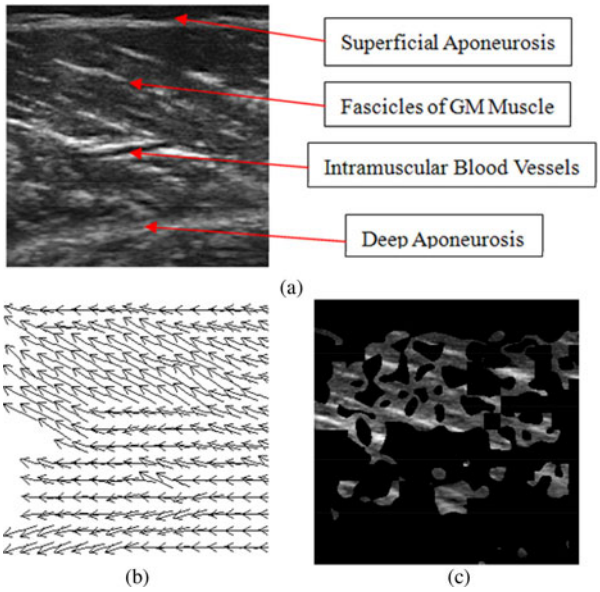

Fig. 3. Example of ultrasound image segmentation with visible intramuscular blood vessels. (a) Original GM ultrasound image with visible intramuscular blood vessels. (b) Orientation flow of the image. (c) Orientation-sensitive segmentation result.

3) *Dominant fascicle orientation estimation*: The dominant fascicle orientation was estimated from all local orientations in the whole image.
4) *Effective fascicle region segmentation*: The image was segmented using the dominant fascicle orientation and a predefined threshold on the local orientation.

1) Normalization: Let $f(x,y)$ denote the gray-level value at pixel (x,y), σ_0 denote the estimated variance of pixel blocks of size $w \times w$ (16×16, in this study), and σ_{img} denote the variance of the whole image. An empirically predefined threshold, $\sigma_T = 0.1\,\sigma_{\mathrm{img}}$, was further used to identify homogeneous regions in the image with

$$H(x,y) = \begin{cases} 1, & \sigma_0 \geq \sigma_T \\ 0, & \text{otherwise.} \end{cases} \tag{1}$$

The mean $\bar{f}$ and variance σ of f were estimated from all pixels having $H(x,y) = 1$. Then, the final normalized gray-level image at pixel (x,y) was defined as follows:

$$f_{\mathrm{norm}}(x,y) = (f(x,y) - \bar{f})/\sqrt{\sigma}. \tag{2}$$

This pixel-wise normalization operation reduced the variations in gray-level values along fascicles but did not change the fascicle structures.

2) Local Orientation Estimation: The local orientation defines invariant coordinates for fascicles in a neighborhood, delineating an inherent property of the structure. Given the normalized image, $f_{\mathrm{norm}}(x,y)$, the estimation of the local orientation field was accomplished as follows.

a) The image $f_{\mathrm{norm}}(x,y)$ was smoothed with a Gaussian filter.
b) The gradients $\partial_x(x,y)$ and $\partial_y(x,y)$ were computed at each pixel using the rotation invariant Scharr operator [45], [46].
c) The image was divided into nonoverlapping blocks Γ of size $w \times w$ to estimate the local orientation of each block centered at pixel (x,y) using the following equations [44]:

$$g_x(x,y) = \sum_{u=x-w/2}^{x+w/2} \sum_{v=y-w/2}^{y+w/2} \partial_x(u,v)\,\partial_y(u,v) \tag{3}$$

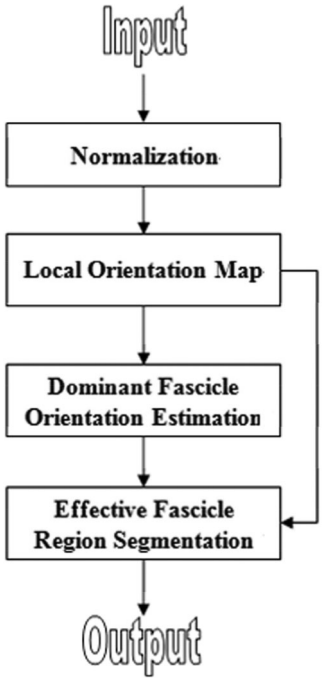

Fig. 4. Flowchart of the proposed segmentation algorithm.

Authorized licensed use limited to: COLORADO SCHOOL OF MINES. Downloaded on July 16,2021 at 21:17:52 UTC from IEEE Xplore. Restrictions apply.

$$g_y(x,y) = \sum_{u=x-w/2}^{x+w/2} \sum_{v=y-w/2}^{y+w/2} \left(\partial_x^2(u,v) - \partial_y^2(u,v)\right) \tag{4}$$

$$\theta(x,y) = \frac{\pi}{2} + \frac{\pi}{2}\tan^{-1}\left(\frac{g_y(x,y)}{g_x(x,y)}\right) \tag{5}$$

where $\theta(x,y)$ is the least-squares estimate of the dominant orientation of the image block centered at pixel (x,y). Since mean fascicle perimeters have been reported to be around 0.8 mm [47], [48], *w* was set to span 1.6 mm, equivalent to 16 pixels for the image resolution of 0.1 mm/pixel used in this study.

d) The reliability of the orientation estimation could also be measured by the reliability coefficient [44]

$$r(x,y) = \frac{\sqrt{\sum_\Gamma \left(\partial_x^2 - \partial_y^2\right) + 4\left(\sum_\Gamma \partial_x \partial_y\right)^2}}{\sum_\Gamma \left(\partial_x^2 + \partial_y^2\right)} \tag{6}$$

which lies in the range [0, 1]. The maximum reliability implies a region having a strongly oriented pattern, with all orientations parallel to each other. In contrast, a minimum coherence means that the region is isotropic.

Using the above steps, a local orientation field estimate and a reliability map could be obtained for the subsequent processing steps. Figs. 2(b) and 3(b) illustrate the local orientation flow map on the GM ultrasound image without and with the visible intramuscular blood vessels [see Figs. 2(a) and 3(a)], respectively.

3) Dominant Orientation Estimation: The reliability measure was used to generate a mask image with a predefined threshold T_r, using

$$M(x,y) = \begin{cases} 1, & r(x,y) \geq T_r \\ 0, & \text{otherwise.} \end{cases} \tag{7}$$

According to the results reported in [49], the threshold T_r was set to be 0.6.

The median value of the local orientations for remaining pixels ($M(x,y) = 1$) was then chosen as the dominant fascicle orientation Θ [49]. This dominant fascicle orientation was then used to identify the effective fascicle region in the subsequent step.

4) Effective Fascicle Region Segmentation: Fascicles were observed to be distributed with similar orientations. The maximum difference of mean fascicle orientation obtained at different muscle sites has been reported to be about 8° [6], [50]. A predefined threshold T_o was then used to segment the effective fascicle region from the whole sequence of ultrasound images. The final effective fascicle region $\Gamma_E(x,y)$ was derived as follows:

$$\Gamma_E(x,y) = \begin{cases} 1, & \text{if } M(x,y) = 1 \text{ and abs}\left(\theta(x,y) - \Theta\right) \leq T_o \\ 0, & \text{otherwise.} \end{cases} \tag{8}$$

This effective fascicle region facilitates fascicle detection, improving the accuracy of fascicle length estimation. According to previous studies [6] and [50], the threshold T_o was empirically determined to be 5°. Figs. 2(c) and 3(c) show an example of the orientation-sensitive segmentation with a threshold T_o of 5° on the GM ultrasound images as shown in Figs. 2(a) and 3(a), respectively.

B. Fascicle Length Estimation With Orientation-Sensitive Segmentation

The fascicles could be identified as straight lines between the superficial and deep aponeuroses. The points on the fascicular path were used to determine the fascicle length from the superficial to the deep aponeuroses, which could be manually defined by identifying the fascicular skeleton in the first frame, and then tracked using the optical flow algorithm for the subsequent frames. Cronin *et al*. [36] determined the fascicle length in a sequence of ultrasound images by applying the Lucas–Kanade optical flow algorithm over a manually selected fascicle region. The six affine transform parameters were first determined from a least-squares fit using the given spatial and temporal gradients over the whole fascicle region between adjacent frames. The affine transform parameters were then applied to derive the displacement of two specific points, $(x_i, y_i), i = 1, 2$, on the fascicular path by adopting the following first-order model:

$$(vx_i, vy_i) = [x_i\ y_i\ 1] \times \begin{bmatrix} d+s1 & s2+r \\ s2-r & d-s1 \\ vxt & vyt \end{bmatrix} \quad i = 1, 2 \tag{9}$$

where the affine flow parameters vxt and vyt are the optical flow at the origin in the *x*- and *y*-directions, respectively, *d* is the rate of dilation, *r* is the rate of rotation, and *s*1 is the shear along the main image axis and *s*2 is the shear along the diagonal axis. The changes of the fascicle length were then obtained from the displacements of these points from one frame to the next.

The *x*- and *y*-grids along with the spatial and temporal gradients were resampled (every 3 pixels) to reduce the computation cost in the least-squares fit [36]. However, the visible nonfascicle components and speckle noise in the selected fascicle region were not taken into account in this resampling method. The spatial and temporal gradients of the nonfascicle components and speckle noise may violate the hypothesis of homogenous affine transformations in the whole fascicle region, which could result in the inaccurate estimation of the global affine flow parameters. Therefore, we proposed a simple and automatic method to calculate the affine transform parameters over the effective fascicle region Γ_E obtained with the orientation-sensitive segmentation in order to achieve both reliable calculation and economic computation cost for the least-squares fitting process. Only the spatial and temporal gradients in Γ_E were applied to calculate the affine transform parameters via a least-squares fit, which could reduce the error caused by the nonfascicle components and speckle noises. The predefined points were then applied to determine the fascicular path by calculating their displacements from the affine transform parameters. Moreover, considering the distribution of aponeuroses in ultrasound images [42], they were recognized using the normalized Radon transform defined

Authorized licensed use limited to: COLORADO SCHOOL OF MINES. Downloaded on July 16,2021 at 21:17:52 UTC from IEEE Xplore. Restrictions apply.

as [51]

$$NR(\rho,\theta) = \frac{\iint I(x,y)\delta(\rho - x\cos\theta - y\sin\theta)dxdy}{L(\rho,\theta)} \quad (10)$$

where $I(x,y)$ is the image intensity at position (x,y), and δ is the Dirac delta function. ρ and θ denote the distance from the center of the image to an arbitrary line and the angle between the x-axis and the line perpendicular to this line, respectively. $L(\rho,\theta)$ represents the length of line (ρ, θ) lying in the ROI. Peaks in $NR(\rho,\theta)$ were identified to detect the position of the aponeuroses using the same strategy introduced in localized Radon transform [32]. Finally, the fascicle length was calculated as the length along the estimated fascicular path from the superficial to the deep aponeuroses.

C. Experiment

Seven adult normal subjects (Age: 34.4 ± 5.0 years; Weight: 66.4 ± 16.2 kg; Body Mass Index: 22.1 ± 4.7 kg/m^2) with no history of musculoskeletal injury were recruited for an experimental study to demonstrate the feasibility of the proposed method. This study was approved by the institutional ethical committee and all subjects signed informed consent prior to participation in the study.

The subject was instructed to stand straight at the beginning of the examination and then conduct the motion of cyclic plantar flexion while keeping the knee angle unchanged. All three-dimensional (3-D) spatial information of their body was obtained from a motion capture system (VICON MX, VICON Corp., Los Angeles, CA, USA). Reflective markers were attached on the subject's left leg with medical proof fabric for recording ankle movement. These reflective markers were placed on the lower lateral surface of the thigh, the lateral and medial epicondyle of the knee, the lower shank, the lateral and medial malleolus, heel, and the first and fifth metatarsal head. A portable ultrasound scanner (SIUI-1100, SIUI Company, Shantou, Guangdong, China) was utilized to simultaneously collect the ultrasound images of the GM with a linear probe. Since the measurements along the midsagittal axis were found to be representative for fascicle measurements both at rest and in the contracted state [6], the probe with a frequency of 5–10 MHz and a field of view of 38 mm was secured steadfastly on the GM midbelly with bandage, and carefully adjusted to visualize fascicles from the superficial to deep aponeuroses with an image resolution of 0.1 mm/pixel and an imaging depth of 4.7 cm. All measurements of the fascicle length were automatically achieved by a custom-designed software developed using Visual Studio (Microsoft, Corporation, Washington, DC, USA). The proposed approach with the orientation-sensitive segmentation, as well as the approach proposed by Cronin *et al.* [36], was applied to estimate the fascicle length in the present study. Moreover, manual measurements of the fascicle length were also performed three times in each image by a single expert who was experienced in ultrasound imaging of muscles and blind to the automatic measurement results. According to the definition of the fascicle length, line segments representing aponeuroses and fascicle were manually drawn in each ultrasound image to obtain an estimate of the fascicle length. The mean value of the manual measurements was used to compare with the automatic measurements. According to Iwanuma *et al.* [52], the ankle angle was also calculated using the 3-D spatial information from the reflective markers to further validate the dynamic measurements.

TABLE I
CMC VALUES BETWEEN THE MANUAL AND AUTOMATIC METHODS FOR THE MEASUREMENT OF THE FASCICLE LENGTH

Subject	CMC value between manual measurement and automatic measurement by the method of Cronin *et al.* (2011) [36]	CMC value between manual measurement and automatic measurement using the proposed method
A	0.97	0.97
B	0.67	0.95
C	0.90	0.95
D	0.92	0.96
E	0.87	0.97
F	0.80	0.98
G	0.96	0.97

D. Data Analysis

Values were reported as mean (±S.D.) for all subjects unless otherwise stated. The manual measurements of the fascicle length were used as reference for comparison with the dynamic measurements. In addition, waveform similarity between the manual and dynamic measurements was assessed by calculating the overall similarity with the coefficient of multiple correlation (CMC) [53], [54]. The CMC was employed as a way of quantifying the percentage variance in fascicle length estimates accounted for within and between the data [53], with a range of 0 and 1. More similar waveforms have higher CMC values, whereas highly dissimilar waveforms can result in a CMC near 0. A Student's paired t-test was applied to test the difference between the CMC values of the proposed method and the approach proposed by Cronin *et al*. [36]. Moreover, a linear regression analysis with zero intercept ($y = kx$; k = regression coefficient) was implemented to describe the relationship between the manual and proposed methods, and a polynomial regression analysis was applied to describe the association between the ankle angle and the fascicle length, considering the viscosity of the fascicles during continuous ankle plantar flexion movement. Pearson product-moment correlations (r) were calculated for the regression analysis. The level of significance was accepted at $p < 0.05$.

III. RESULTS

As shown in Table I, the CMC value (0.87 ± 0.1) determined by Cronin's approach ranged from 0.67 to 0.97, while the proposed method had CMC value (0.97 ± 0.01) ranging from 0.95 to 0.98. The difference in the CMC value between these two methods was significant ($p = 0.048$). Fig. 5 shows the changes of the fascicle length in the GM images without nonfascicle components during cyclic plantar flexion for one typical subject. The high-CMC values suggested a good agreement between the

Authorized licensed use limited to: COLORADO SCHOOL OF MINES. Downloaded on July 16,2021 at 21:17:52 UTC from IEEE Xplore. Restrictions apply.

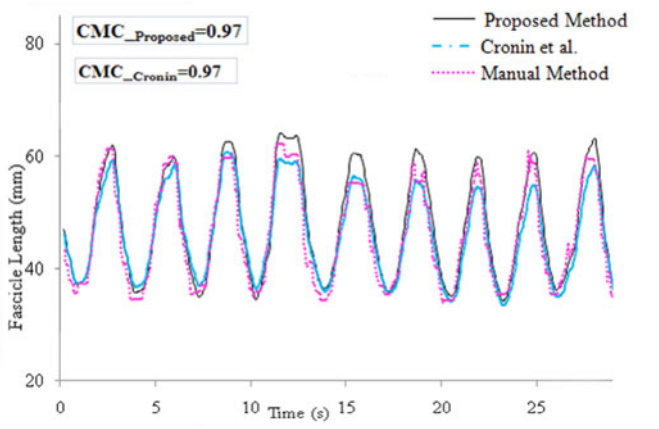

Fig. 5. Change of fascicle length obtained with the proposed method, the approach proposed by Cronin *et al*. [36], and the manual method during plantar flexion for subject A.

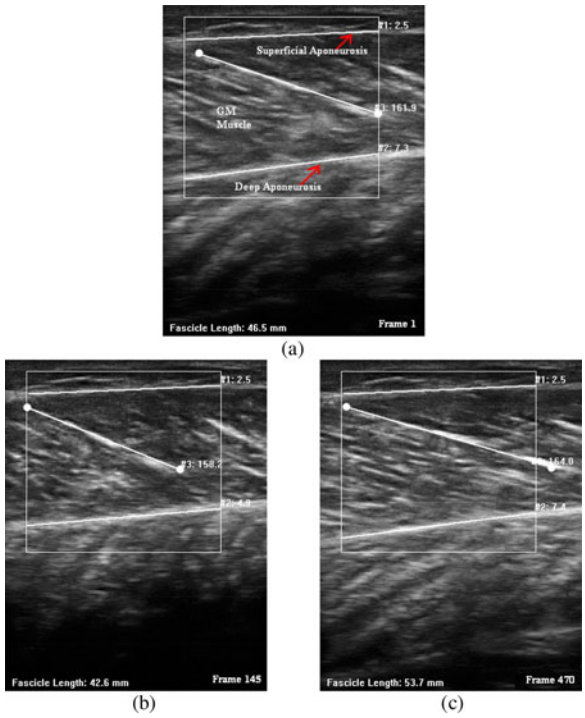

Fig. 6. Measurement of the fascicle length for subject A using the approach proposed by Cronin *et al*. [36]. (a) Fascicle in the first frame manually defined with the fascicle end points (white circles). (b) Measurement of the fascicle length at frame 145. (c) Measurement of the fascicle length at frame 470.

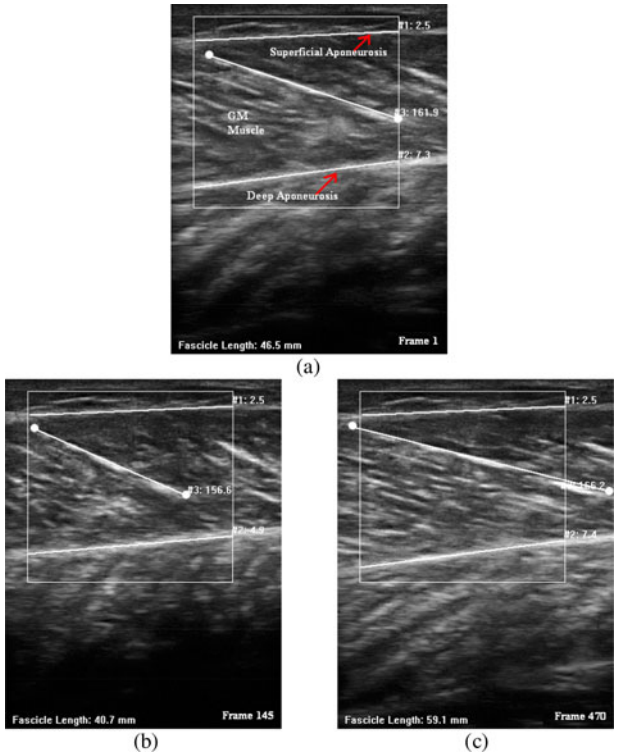

Fig. 7. Measurement of the fascicle length for subject A using the proposed approach. (a) Fascicle in the first frame manually defined with the fascicle end points (white circles). (b) Measurement of the fascicle length at frame 145. (c) Measurement of the fascicle length at frame 470.

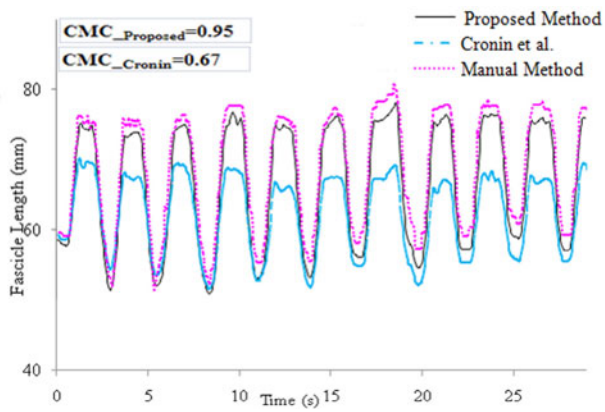

Fig. 8. Change of fascicle length obtained with the proposed method, the approach proposed by Cronin *et al*. [36], and the manual method during plantar flexion for subject B.

manual and dynamic measurements for both the proposed and Cronin's methods. These results demonstrated the comparable performance between the two methods when dealing with a sequence of ultrasound images without nonfascicle components. As shown in Figs. 6 and 7, the fascicular path determined by Cronin's approach in comparison with the proposed approach exhibited slight deviation from the actual, targeted fascicle in some frames, which can be ascribed to speckle noise. Even worse, the changes in orientation and location of the fascicles could not be accurately estimated using the affine transform parameters estimated from the whole fascicle patch when non-fascicle components were observed in the images. Fig. 8 shows a typical example of the fascicle length measured with the proposed approach, for which Cronin's method failed to track the change in fascicles. As shown in Fig. 9(b), the target points deviated from the predefined fascicular path due to the visible intramuscular blood vessels, and this deviation was accumulated in subsequent frames [see Fig. 9(c)]. Since the fascicle structures in the image were not taken into account, such errors could not be avoided when the whole fascicle region was used to estimate the affine transform parameters. On the other hand,

Authorized licensed use limited to: COLORADO SCHOOL OF MINES. Downloaded on July 16,2021 at 21:17:52 UTC from IEEE Xplore. Restrictions apply.

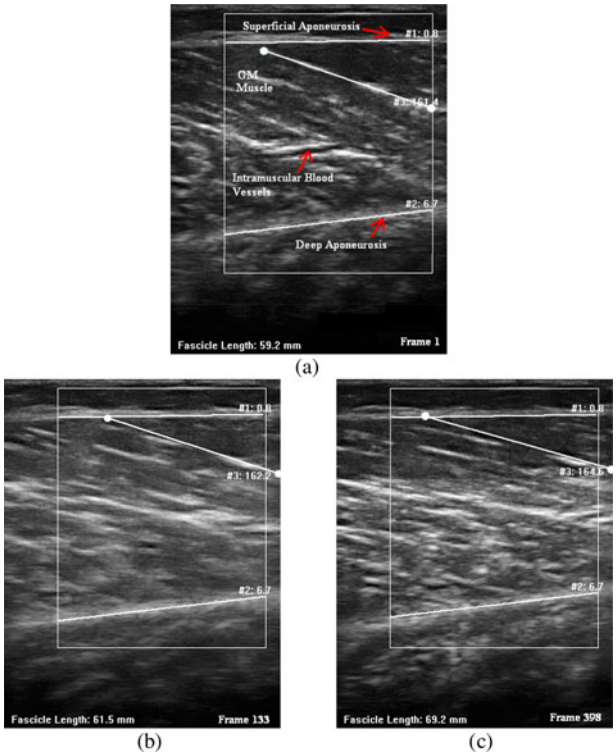

Fig. 9. Measurement of the fascicle length for subject B using the approach proposed by Cronin *et al*. [36]. (a) Fascicle in the first frame manually defined with the fascicle end points (white circles). (b) Measurement of the fascicle length at frame 133. (c) Measurement of the fascicle length at frame 398.

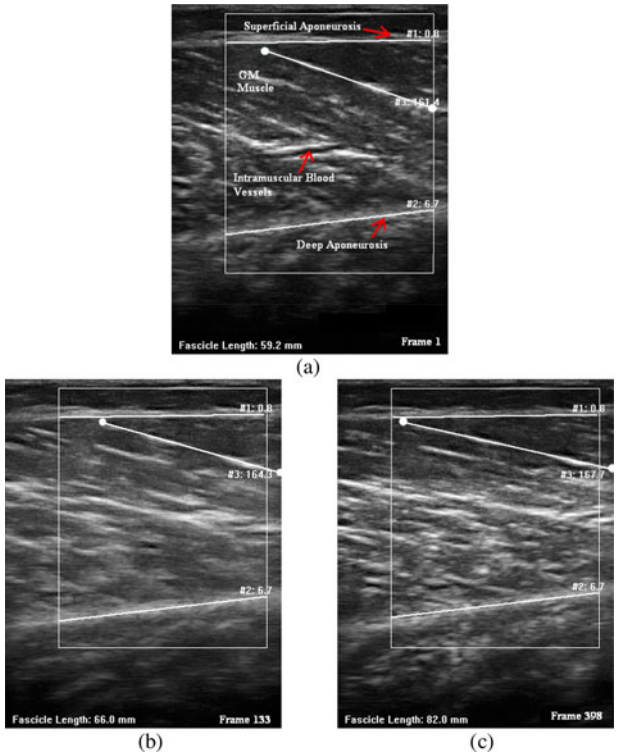

Fig. 10. Measurement of the fascicle length for subject B using the proposed approach. (a) Fascicle in the first frame manually defined with the fascicle end points (white circles). (b) Measurement of the fascicle length at frame 133. (c) Measurement of the fascicle length at frame 398.

our proposed tracking approach only used the effective fascicle region to calculate the affine transform parameters, thus avoiding the influence of nonfascicle components and speckle noise [see Fig. 10(b) and (c)]. The CMC values also suggested that the dynamic measurement with the proposed method was more consistent with the manual measurement compared with Cronin's approach. Moreover, the results revealed a positive linear correlation between the proposed method and the manual measurement ($r = 0.94 \pm 0.04$; all $p < 0.001$; see Table II), and the average regression coefficient (slope) between the manual measurements and the proposed method (slope $= 0.99 \pm 0.03$) was close to 1.0. These results support the conclusion that the proposed approach was reliable for the estimation of the fascicle length. When the plantar flexion angle was increased to $33.1 \pm 5.0°$, the fascicle length measured with the proposed method was shortened from 70.4 ± 6.8 mm to 39.3 ± 8.8 mm, and was negatively correlated with the ankle joint angle ($r = -0.93 \pm 0.02$, all $p < 0.001$). In addition, the average computation time for the estimation of the fascicle length with the proposed method in the $\sim 300 \times 300$ pixel ROI was about $4 \sim 5$ s for each frame using a computer with an Intel Core 2 Q8400 2.66-GHz processor and 2048 MB of memory.

TABLE II
LINEAR REGRESSION ANALYSIS BETWEEN THE MANUAL AND PROPOSED METHOD FOR THE MEASUREMENT OF THE FASCICLE LENGTH

Subject	Regression coefficient (slope) between manual and automatic measurements of fascicle length	Correlation between manual and automatic measurements of fascicle length
A	1.04	0.96 ($p < 0.001$)
B	0.94	0.98 ($p < 0.001$)
C	1.00	0.86 ($p < 0.001$)
D	1.00	0.92 ($p < 0.001$)
E	1.00	0.95 ($p < 0.001$)
F	1.00	0.96 ($p < 0.001$)
G	0.96	0.96 ($p < 0.001$)

IV. DISCUSSION

The proposed orientation-sensitive segmentation algorithm utilized prior knowledge of the geometric arrangement of fascicles to identify the effective fascicle region from ultrasound images, which can therefore be applied as a preprocessing step for the estimation of the fascicle length. The Lucas–Kanade optical flow algorithm over the effective fascicle region rendered the estimation of global affine transform parameters more reliable, since it obviated the influence of nonfascicle components and speckle noise on the motion estimation of points on the fascicular path. The preliminary results demonstrated that the proposed method could reliably track the change of the fascicle length in continuous ultrasound images, which were in good agreement with those obtained by manual measurement and correlated well with kinematic data, such as the ankle angle.

The affine flow parameters estimated over the whole fascicle region avoided the accumulation of small errors caused by tracking a small ROI [38]. However, this approach could still exhibit a tracking error due to inhomogeneous deformation across the

Authorized licensed use limited to: COLORADO SCHOOL OF MINES. Downloaded on July 16,2021 at 21:17:52 UTC from IEEE Xplore. Restrictions apply.

region of interest between consecutive images, as demonstrated using Cronin's approach (CMC $= 0.87 \pm 0.10$), which may be due to the nonfascicle components and speckle noise. The spatial and temporal gradients of the nonfascicle components and speckle noise made the estimation of global affine transform parameters imprecise, resulting in accumulated tracking errors. Moreover, it was observed that the deformation of nonfascicle components, such as intramuscular blood vessels, was usually inconsistent with that of the fascicles, which contributed to the incorrect estimations using Cronin's approach. On the other hand, the proposed method using orientation-sensitive segmentation may eliminate the contribution from nonfascicle components and speckle noise in the estimation of global affine flow parameters, because it segments visible fascicle structures from the whole image for the calculation of global affine transform parameters. The overall high CMC value (0.97 ± 0.01) and very close regression ($r = 0.94 \pm 0.04$; slope $= 0.99 \pm 0.03$) demonstrated that the results of the proposed method were consistent with the manual measurements. Moreover, the significantly larger CMC value for the proposed method ($p = 0.048$), compared with Cronin's approach, suggested that this method had a better performance in tracking fascicles, thus was more robust in the measurement of the fascicle length. Additionally, the processing time is currently between 4 and 5 s/frame, making real-time application possible. The computational time may even be further greatly reduced, since block-wise calculation in the effective fascicle region can be processed by parallel computation techniques using a graphics processing unit (GPU).

The changes and values of fascicle lengths measured with the proposed method were consistent with previous reports [7], [25], and [55]. In this study, the average fascicle length for an ankle angle of 0° was 70.4 ± 6.8 mm, and was reduced to 39.3 ± 8.8 mm with the plantar flexion angle reaching $33.1 \pm 5.0°$. The average absolute values of maximum and minimum fascicle length were reported to be 71 and 64 mm during the stance phase [55]. The fact that the GM fascicles maintained a near-constant length around the plateau region of the force–length curve has been reported when the muscle was active during a major part of stance in walking [24]. The shortest mean GM fascicle length for walking and running has been reported to be 44.1 ± 1.0 mm and 40.1 ± 0.6 mm, respectively [25]. The high correlation between the ankle angle and fascicle length ($r = -0.93 \pm 0.02$; all $p < 0.001$) found in this study also suggested that the fascicle length is dependent on the ankle joint angle, in agreement with the previous reports [7] and [17]. As the ankle angle increased to 30°, the GM fascicle length was shortened by about 32% at rest [7]. In addition, the muscle size in elderly humans, including the fascicle length, is known to be enlarged with resistive training programs [56]. This finding indicates an increase in the number of sarcomeres in series, resulting in a larger force generation capability [21]. Therefore, it is feasible to generalize the use of the fascicle length into whole motion analysis with the proposed method, which would facilitate an improved understanding of the architectural and bioelectrical properties of muscle.

Nonetheless, the method proposed in this study still had some limitations. First, it was assumed that the fascicles being tracked conform to homogeneous affine transformations. This assumption may not hold in some movement tasks where changes in the local muscle shape instead of global shape are more of interest [36], making this approach unreliable. The initialization may also affect the estimation accuracy of the fascicle length. Moreover, although the fascicle structures had been taken into account in our method, it still lacked the ability to examine possible tracking errors by identifying individual fascicles. Furthermore, a two-point fascicle representation may not properly account for the fascicle curvature. Fascicles are nearly straight at rest, as the contraction level increases, fascicles become slightly curved and muscle length decreases, resulting in an approximately 6% underestimation of the fascicle length during a maximum voluntary contraction [57]. Thus, this effect is likely to be a minor factor in measuring the fascicle length in human daily dynamic tasks. Nevertheless, it would be ideal if the algorithm was able to track multiple points along a fascicle for curvature measurement in future.

V. Conclusion

We have successfully developed a new approach using orientation-sensitive segmentation for automatically estimating the fascicle length in a series of ultrasound images utilizing prior knowledge of the orientations of fascicles. The orientation-sensitive segmentation algorithm precluded the influence of nonfascicle components on the calculation of affine transform parameters, resulting in a more reliable measurement of the fascicle length. The results obtained using the proposed approach showed good agreement with those obtained by manual measurements. The method therefore provides an alternative dynamic measurement of muscle activation with ultrasound imaging to analyze the muscle function in human motion analysis. Future studies with a large group of subjects and other types of motion such as walking will be conducted to further demonstrate the potential of this new method for full understanding of muscle activation. The performance of the newly proposed method can also be further enhanced by using GPU programming to achieve real-time application in future studies.

References

[1] V. M. Zatsiorsky and B. I. Prilutsky, *Biomechanics of Skeletal Muscles*. Champaign, IL, USA: Human Kinetics, 2012.
[2] Y. P. Zheng *et al.*, "Sonomyography: Monitoring morphological changes of forearm muscles in actions with the feasibility for the control of powered prosthesis," *Med. Eng. Phys.*, vol. 28, no. 5, pp. 405–415, Jun. 2006.
[3] G. R. Adams *et al.*, "Magnetic resonance imaging and electromyography as indexes of muscle function," *J. Appl. Physiol.*, vol. 73, no. 4, pp. 1578–1589, Oct. 1992.
[4] G. R. Adams *et al.*, "Mapping of electrical muscle stimulation using MRI," *J. Appl. Physiol.*, vol. 74, no. 2, pp. 532–537, Feb. 1993.
[5] C. J. Zuurbier and P. A. Huijing, "Changes in geometry of actively shortening unipennate rat gastrocnemius muscle," *J. Morphol.*, vol. 218, no. 2, pp. 167–80, Nov. 1993.
[6] M. V. Narici *et al.*, "In vivo human gastrocnemius architecture with changing joint angle at rest and during graded isometric contraction," *J. Physiol.*, vol. 496, no. 1, pp. 287–297, Oct. 1996.
[7] C. N. Maganaris *et al.*, "In vivo measurements of the triceps surae complex architecture in man: Implications for muscle function," *J. Physiol.*, vol. 512, no. 2, pp. 603–614, Oct. 15, 1998.
[8] P. W. Hodges *et al.*, "Measurement of muscle contraction with ultrasound imaging," *Muscle Nerve*, vol. 27, no. 6, pp. 682–692, Jun. 2003.

Authorized licensed use limited to: COLORADO SCHOOL OF MINES. Downloaded on July 16,2021 at 21:17:52 UTC from IEEE Xplore. Restrictions apply.

[9] K. Manal *et al.*, "Can pennation angles be predicted from EMGs for the primary ankle plantar and dorsiflexors during isometric contractions?" *J. Biomechanics*, vol. 41, no. 11, pp. 2492–2497, Aug. 2008.

[10] A. A. Mohagheghi *et al.*, "In vivo gastrocnemius muscle fascicle length in children with and without diplegic cerebral palsy," *Dev. Med. Child Neurol.*, vol. 50, no. 1, pp. 44–50, Jan. 2008.

[11] L. Barber *et al.*, "Medial gastrocnemius muscle fascicle active torque-length and Achilles tendon properties in young adults with spastic cerebral palsy," *J. Biomechanics*, vol. 45, no. 15, pp. 2526–2530, Oct. 2012.

[12] K. Reardon *et al.*, "Quadriceps muscle wasting persists 5 months after total hip arthroplasty for osteoarthritis of the hip: A pilot study," *Internal Med. J.*, vol. 31, no. 1, pp. 7–14, Jan.-Feb., 2001.

[13] C. Suetta *et al.*, "Resistance training induces qualitative changes in muscle morphology, muscle architecture, and muscle function in elderly postoperative patients," *J. Appl. Physiol.*, vol. 105, no. 1, pp. 180–186, Jul. 2008.

[14] X. Chen *et al.*, "Sonomyography (SMG) control for powered prosthetic hand: A study with normal subjects," *Ultrasound Med. Biol.*, vol. 36, no. 7, pp. 1076–1088, Jul. 2010.

[15] J. Y. Guo *et al.*, "Towards the application of one-dimensional sonomyography for powered upper-limb prosthetic control using machine learning models," *Prosthetics Orthotics Int.*, vol. 37, no. 1, pp. 43–49, Feb. 2013.

[16] T. Fukunaga *et al.*, "Determination of fascicle length and pennation in a contracting human muscle in vivo," *J. Appl. Physiol.*, vol. 82, no. 1, pp. 354–358, Jan. 1997.

[17] Y. Kawakami *et al.*, "Architectural and functional features of human triceps surae muscles during contraction," *J. Appl. Physiol.*, vol. 85, no. 2, pp. 398–404, Aug. 1998.

[18] M. V. Narici *et al.*, "Ageing of human muscles and tendons," *Disability Rehabil.*, vol. 30, no. 20–22, pp. 1548–1554, 2008.

[19] M. V. Narici *et al.*, "Effect of aging on human muscle architecture," *J. Appl. Physiol.*, vol. 95, no. 6, pp. 2229–2234, Dec. 2003.

[20] L. Mademli and A. Arampatzis, "Behaviour of the human gastrocnemius muscle architecture during submaximal isometric fatigue," *Eur. J. Appl. Physiol.*, vol. 94, no. 5–6, pp. 611–617, Aug. 2005.

[21] J. Duclay *et al.*, "Behavior of fascicles and the myotendinous junction of human medial gastrocnemius following eccentric strength training," *Muscle Nerve*, vol. 39, no. 6, pp. 819–827, Jun. 2009.

[22] A. J. Blazevich, "Effects of physical training and detraining, immobilisation, growth and aging on human fascicle geometry," *Sports Med.*, vol. 36, no. 12, pp. 1003–1017, 2006.

[23] T. Fukunaga *et al.*, "In vivo behaviour of human muscle tendon during walking," *Proc. Roy. Soc. B—Biological Sci.*, vol. 268, no. 1464, pp. 229–233, Feb. 2001.

[24] T. Fukunaga *et al.*, "Muscle and tendon interaction during human movements," *Exercise Sport Sci. Rev.*, vol. 30, no. 3, pp. 106–110, Jul. 2002.

[25] G. A. Lichtwark and A. M. Wilson, "Interactions between the human gastrocnemius muscle and the Achilles tendon during incline, level and decline locomotion," *J. Exp. Biol.*, vol. 209, no. 21, pp. 4379–4388, Nov. 2006.

[26] A. Ishikawa *et al.*, "Medial gastrocnemius muscle behavior during human running and walking," *Gait Posture*, vol. 25, no. 3, pp. 380–384, Mar. 2007.

[27] D. J. Farris and G. S. Sawicki, "Human medial gastrocnemius force-velocity behavior shifts with locomotion speed and gait," *Proc. Nat. Acad. Sci. United States Amer.*, vol. 109, no. 3, pp. 977–982, Jan. 2012.

[28] N. Aggeloussis *et al.*, "Reproducibility of fascicle length and pennation angle of gastrocnemius medialis in human gait in vivo," *Gait Posture*, vol. 31, no. 1, pp. 73–77, Jan. 2010.

[29] G. P. Pappas *et al.*, "Nonuniform shortening in the biceps brachii during elbow flexion," *J. Appl. Physiol.*, vol. 92, no. 6, pp. 2381–2389, Jun. 1, 2002.

[30] Y. J. Zhou and Y. P. Zheng, "Estimation of muscle fiber orientation in ultrasound images using revoting Hough transform (RVHT)," *Ultrasound Med. Biol.*, vol. 34, no. 9, pp. 1474–1481, Sep. 2008.

[31] M. Rana *et al.*, "Automated tracking of muscle fascicle orientation in B-mode ultrasound images," *J. Biomechanics*, vol. 42, no. 13, pp. 2068–2073, Sep. 2009.

[32] H. Zhao and L. Q. Zhang, "Automatic tracking of muscle fascicles in ultrasound images using localized radon transform," *IEEE Trans. Biomed. Eng.*, vol. 58, no. 7, pp. 2094–2101, Jul. 2011.

[33] S. Bianchi *et al.*, *Ultrasound of the Musculoskeletal System*. New York, NY, USA: Springer, 2007.

[34] J. Darby *et al.*, "Automated regional analysis of B-mode ultrasound images of skeletal muscle movement," *J. Appl. Physiol.*, vol. 112, no. 2, pp. 313–327, Jan. 2012.

[35] I. D. Loram *et al.*, "Use of ultrasound to make noninvasive in vivo measurement of continuous changes in human muscle contractile length," *J. Appl. Physiol.*, vol. 100, no. 4, pp. 1311–1323, Apr. 2006.

[36] N. J. Cronin *et al.*, "Automatic tracking of medial gastrocnemius fascicle length during human locomotion," *J. Appl. Physiol.*, vol. 111, no. 5, pp. 1491–1496, Nov. 2011.

[37] J. Darby *et al.*, "Estimating skeletal muscle fascicle curvature from B-mode ultrasound image sequences," *IEEE Trans. Biomed. Eng.*, vol. 60, no. 7, pp. 1935–1945, Jul. 2013.

[38] J. G. Gillett *et al.*, "Reliability and accuracy of an automated tracking algorithm to measure controlled passive and active muscle fascicle length changes from ultrasound," *Comput. Methods Biomechanics Biomed. Eng.*, vol. 16, no. 6, pp. 678–687, Jun. 2013.

[39] B. D. Lucas and T. Kanade, "An iterative image registration technique with an application to stereo vision," in *Proc. 7th Int. Joint Conf. Artif. Intell.*, Vancouver, BC, Canada, 1981, vol. 2, pp. 674–679.

[40] J. Shi and C. Tomasi, "Good features to track," in *Proc. IEEE Comput. Soc. Conf. Comput. Vision Pattern Recog.*, 1994, pp. 593–600.

[41] A. F. Frangi *et al.*, "Multiscale vessel enhancement filtering," in *Medical Image Computing and Computer-Assisted Intervention*, W. M. Wells, A. Colchester, and S. Delp, Eds. Berlin: Springer-Verlag Berlin, 1998, pp. 130–137.

[42] S. Bianchi and C. Martinoli, *Ultrasound of the Musculoskeletal System*, Berlin, Germany: Springer, 2007.

[43] L. Hong *et al.*, "Fingerprint image enhancement: Algorithm and performance evaluation," *IEEE Trans. Pattern Anal. Mach. Intell.*, vol. 20, no. 8, pp. 777–789, Aug. 1998.

[44] A. R. Rao, *A Taxonomy for Texture Description and Identification*. Berlin, Germany: Springer-Verlag, 1990.

[45] H. Scharr, "Optimal filters for extended optical flow," in *Complex Motion*, B. Jähne, R. Mester, E. Barth, and H. Scharr, Eds. Berlin, Germany: Springer, 2007, pp. 14–29.

[46] J. Weickert and H. Scharr, "A scheme for coherence-enhancing diffusion filtering with optimized rotation invariance," *J. Vis. Commun. Image R.*, vol. 13, no. 1-2, pp. 103–118, Mar-Jun 2002.

[47] P. E. Williams *et al.*, "Relationship between fascicle size and perineurial collagen IV content in diabetic and control human peripheral nerve," *Histopathology*, vol. 36, no. 6, pp. 551–555, Jun. 2000.

[48] R. T. Kohrs *et al.*, "Tendon fascicle gliding in wild type, heterozygous, and lubricin knockout mice," *J. Orthopaedic Res.*, vol. 29, no. 3, pp. 384–389, 2011.

[49] Y. J. Zhou, J. Z. Li, G. Q. Zhou, *et al.*, "Dynamic measurement of pennation angle of gastrocnemius muscles during contractions based on ultrasound imaging," *Biomed. Eng. Online*, vol. 11, p. 63, (Sep. 2012). [Online]. Available: http://www.biomedical-engineering-online.com/content/11/1/63

[50] R. D. Herbert *et al.*, "Changes in the length and three-dimensional orientation of muscle fascicles and aponeuroses with passive length changes in human gastrocnemius muscles," *J. Physiol.*, vol. 593, pp. 441–455, Jan. 2015.

[51] G.-Q. Zhou *et al.*, "Automatic measurement of pennation angle and fascicle length of gastrocnemius muscles using real-time ultrasound imaging," *Ultrasonics*, vol. 57, pp. 72–83, Mar. 2015.

[52] S. Iwanuma *et al.*, "Triceps surae muscle-tendon unit length changes as a function of ankle joint angles and contraction levels: The effect of foot arch deformation," *J. Biomechanics*, vol. 44, no. 14, pp. 2579–2583, Sep. 2011.

[53] M. P. Kadaba *et al.*, "Repeatability of kinematic, kinetic, and electromyographic data in normal adult gait," *J. Orthopaedic Res.*, vol. 7, no. 6, pp. 849–860, Nov. 1989.

[54] J. J. Kavanagh *et al.*, "Reliability of segmental accelerations measured using a new wireless gait analysis system," *J. Biomechanics*, vol. 39, no. 15, pp. 2863–2872, 2006.

[55] O. S. Mian *et al.*, "Gastrocnemius muscle-tendon behaviour during walking in young and older adults," *Acta Physiologica*, vol. 189, no. 1, pp. 57–65, Jan. 2007.

[56] N. D. Reeves *et al.*, "Effect of resistance training on skeletal muscle-specific force in elderly humans," *J. Appl. Physiol.*, vol. 96, no. 3, pp. 885–892, Mar. 2004.

[57] T. Muramatsu *et al.*, "In vivo determination of fascicle curvature in contracting human skeletal muscles," *J. Appl. Physiol.*, vol. 92, no. 1, pp. 129–134, Jan. 2002.

Authors' photographs and biographies not available at the time of publication.

Authorized licensed use limited to: COLORADO SCHOOL OF MINES. Downloaded on July 16,2021 at 21:17:52 UTC from IEEE Xplore. Restrictions apply.